

## Crystalline Amorphous Semiconductor Superlattice

T. C. Chong,<sup>1,2</sup> L. P. Shi,<sup>1,\*</sup> X. Q. Wei,<sup>1,2</sup> R. Zhao,<sup>1</sup> H. K. Lee,<sup>1</sup> P. Yang,<sup>3</sup> and A. Y. Du<sup>4</sup>

<sup>1</sup>Data Storage Institute, A\*STAR (Agency for Science, Technology and Research), Singapore 117608

<sup>2</sup>Electrical Computer Engineering Department, National University of Singapore, Singapore 117576

<sup>3</sup>Singapore Synchrotron Light Source (SSLS), National University of Singapore, Singapore 117603

<sup>4</sup>Institute of Microelectronics, A\*STAR (Agency for Science, Technology and Research), Singapore 117685

(Received 12 September 2007; published 31 March 2008)

A new class of superlattice, crystalline amorphous superlattice (CASL), by alternatively depositing two semiconductor materials, is proposed. CASL displays three states depending on the component materials' phase: both polycrystalline phases, both amorphous phases, and one polycrystalline phase while another amorphous phase. Using materials capable of reversible phase transition, CASL can demonstrate reversibility among three states. GeTe/Sb<sub>2</sub>Te<sub>3</sub> CASL has been synthesized and proved by x-ray reflectometry and TEM results. The reversible transition among three states induced by electrical and laser pulse was observed. The changes in the optical absorption edge, electrical resistivity, thermal conductivity, and crystallization temperature as a function of layer thickness are interpreted as quantum or nanoeffects. The unique properties of CASL enable the design of materials with specific properties.

DOI: [10.1103/PhysRevLett.100.136101](https://doi.org/10.1103/PhysRevLett.100.136101)

PACS numbers: 68.65.Cd, 61.43.Dg, 68.35.Rh, 73.21.Cd

Semiconductor superlattice (SL) exhibits many attractive electrical, optical and thermal properties which are associated with the periodic nature of SL and the repeat distance in the structure, such as quantum size effects [1]. Two classes of SLs, crystalline SL and amorphous SL, have been demonstrated and studied, respectively. Crystalline SL was the first to be produced. The matching of the lattice constants of the individual layers is the crucial requirement in fabrication of crystalline SL which restricts the number of materials to form SLs. However, such strict requirement can be relaxed in amorphous SL due to amorphous structure by its very own nature [2]. It has been demonstrated that uniformed multilayer of amorphous semiconductor can be fabricated with very thin component layer of sharp interfaces. Compared to crystalline SL, amorphous SL has much more freedom in choosing components of the SL structures as there is no limitation by the lattice matching condition.

In this Letter, we propose and synthesize a third class of SL, crystalline-amorphous superlattices (CASL). CASL consists of two semiconductor materials which are alternatively deposited. The component materials could be either polycrystalline or amorphous phase. Depending on the phase of the component materials, CASL displayed three different states: both in amorphous phases demonstrating an amorphous SL (*a*-CASL); both in polycrystalline phases demonstrating a crystalline SL (*c*-CASL); one in polycrystalline phase while the other one in amorphous phase, thus demonstrating a mix of amorphous and crystalline SL (*m*-CASL). The key to fabricating CASL is to form defect free interface which is highly dependent on the properties of the component materials, such as lattice constant, bonding, adhesion force, etc. In order to realize *m*-CASL state, it is desirable for the component materials

to have a large difference in their crystallization temperatures  $T_x(c)$ . If the component materials are chosen appropriately, for example, chalcogenide materials which can realize reversible transition between amorphous and crystalline phases, CASL is capable of a reversible transition among the three states by using different means, e.g., electrical or laser pulse. The reversible phase transition in chalcogenide materials is due to the fact that the top of the valence band consists of lone-pair orbits with lone-pair electron and hole. Also the localized states in the gap are caused by the interactions between lone-pair electrons on different atoms and interactions with their local environment [3,4].

In this work, CASL was fabricated on Si substrate using binary compounds of GeTe and Sb<sub>2</sub>Te<sub>3</sub> as the two component materials. Sb<sub>2</sub>Te<sub>3</sub> has a rhombohedral lattice of the tetradymite (Bi<sub>2</sub>Te<sub>2</sub>S) type in the hexagonal configuration with lattice parameters:  $a = 0.4264$  nm,  $c = 3.0453$  nm. For GeTe, there are two polymorphic phases. The high temperature  $\beta$  phase ( $T > 700$  K) has a cubic rocksalt structure. The low temperature  $\alpha$  phase ( $T < 700$  K) has a rhombohedral structure of the  $\alpha$ -As type with lattice parameters:  $a = 0.5986$  nm and  $\alpha = 88.35^\circ$ . The activation energy of GeTe and Sb<sub>2</sub>Te<sub>3</sub> is 0.39 and 0.28 eV, respectively [5,6]. The Sb<sub>2</sub>Te<sub>3</sub> and GeTe thin films were prepared by ion beam deposition system, Roth & Rau IonSys 1000. The base pressure was initially  $3 \times 10^{-8}$  mbar. During deposition, a microwave power of 243 W at 2.45 GHz, a beam voltage of 800 V and an accelerator voltage of  $-600$  V were applied. Using Ar at a flow rate of 4 sccm, the pressure was increased to  $9.2 \times 10^{-5}$  mbar. Sb<sub>2</sub>Te<sub>3</sub> and GeTe were then deposited at rates of 7.3 and 2.5 nm/min respectively. Each component layer was deposited alternatively with the same thickness varying from

1 to 20 nm. The thickness of a pair of GeTe/Sb<sub>2</sub>Te<sub>3</sub> layers is called a period in this Letter. For the CASL sample, 40 periods were grown.

GeTe/Sb<sub>2</sub>Te<sub>3</sub> CASL crystalline structure was characterized by x-ray diffractometry using CuK $\alpha$ <sub>1</sub> radiation. For the as-deposited sample, no peak was observed, indicating that both GeTe and Sb<sub>2</sub>Te<sub>3</sub> were at amorphous phase. When the sample was heated to 100 °C in vacuum for 5 minutes, a peak at 36.7° was observed, indicating that Sb<sub>2</sub>Te<sub>3</sub> layer had crystallized. No peak for polycrystalline GeTe was observed, indicating that GeTe remained in amorphous phase. The state was a *m*-CASL. When the sample was further heated to 200 °C, an additional peak at 25.90° appeared which showed the existence of polycrystalline GeTe and Sb<sub>2</sub>Te<sub>3</sub>. The CASL was then a *c*-CASL.

The three states were confirmed by x-ray reflectometry (XRR) as shown in Fig. 1. The CASL period was designed to be 7 nm, and the 40 periods grown were capped with 4.3 nm thick ZnS-SiO<sub>2</sub> layer. From Fig. 1, it can be seen that the three states all exhibit sharp satellite diffraction peaks. The full width at half-maximum (FWHM) of the diffraction peak on the diffraction angle  $\theta$  bears the information on the interfacial abruptness. For *a*-CASL, FWHM is 0.07° for the peak at  $\theta = 0.645^\circ$ , which corresponds to a period of 7.73 nm. It shows that a well-defined amorphous SL was obtained at *a*-CASL state; for *m*-CASL, FWHM is 0.07° for the peak at  $\theta = 0.652^\circ$ . The increase of the peak angle is due to the decrease in period to 7.62 nm and increase in Sb<sub>2</sub>Te<sub>3</sub> density from 6.05 to 6.26 g/cm<sup>3</sup> during the crystallization; For *c*-CASL FWHM is 0.05° for the peak at  $\theta = 0.688^\circ$  which corresponds to a period of

7.13 nm. It reveals that the period of *c*-CASL is the smallest. After fitting the XRR data, the density was found to increase from 6.05 to 6.44 g/cm<sup>3</sup> for Sb<sub>2</sub>Te<sub>3</sub> and from 5.10 to 5.33 g/cm<sup>3</sup> for GeTe. These results show that the density of crystalline phase is larger than that of amorphous phase. The small FWHM for the three peaks showed that well-defined SL has been obtained in all three states of CASL.

The existence of well-defined layers for GeTe/Sb<sub>2</sub>Te<sub>3</sub> CASL was also confirmed by TEM. The individual layer thickness was found to be matched with that obtained by XRR. The roughness of the interface is less than 1 nm.

It has been well accepted that the resistance or reflection difference can be used to identify the difference between amorphous and crystalline phases [7,8]. In this work, the reversible transitions among the three states of GeTe/Sb<sub>2</sub>Te<sub>3</sub> CASL have been realized by applying electrical and laser pulses, respectively. The reversible transitions induced by laser pulse have been observed by measuring three reflection levels with a setup reported in Ref. [8]. Because of the length limit of the Letter, the results of state transition by electrical pulse are presented only. The reversible transition between amorphous and crystalline phases has been observed by the switching between the high and low resistances for both GeTe and Sb<sub>2</sub>Te<sub>3</sub> [7,9]. The resistance difference can be used to identify *c*-CASL, *m*-CASL, and *a*-CASL with *c*-CASL and *a*-CASL having the lowest and highest resistance, respectively.

To enable electrical testing, electrodes were formed on the top and bottom of CASL. Figure 2 shows the resistance

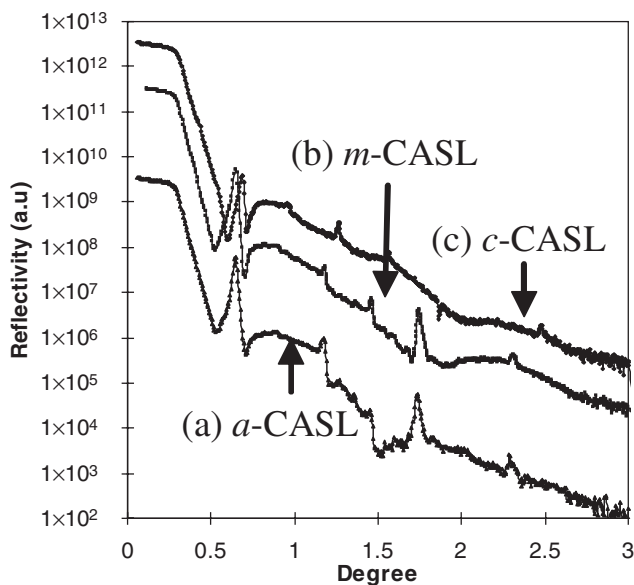


FIG. 1. XRR measurement results of the sample (a) as-deposited, heated to (b) 100 °C, and (c) 200 °C in vacuum for 5 min.

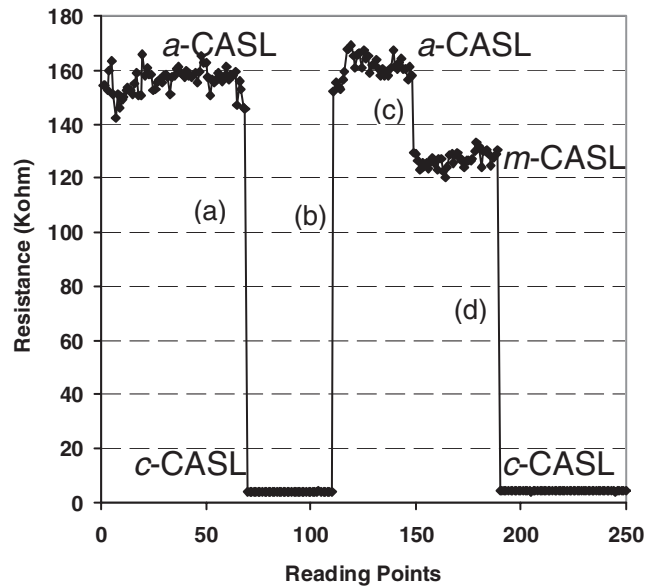


FIG. 2. Resistance changes among the three states of GeTe/Sb<sub>2</sub>Te<sub>3</sub> CASL induced by electric pulses, (a) *a*-CASL to *c*-CASL, (b) *c*-CASL to *a*-CASL, (c) *a*-CASL to *m*-CASL, and (d) *m*-CASL to *c*-CASL.

changes induced by electrical pulses. When an electrical pulse of 200 ns and 0.8 V was applied, CASL changed from initial *a*-CASL to *c*-CASL, (a) in Fig. 2, which is indicated by the sharp drop in the measured resistance value. When an electrical pulse of 40 ns and 2 V was subsequently applied, CASL changed back from *c*-CASL to *a*-CASL directly, (b) in Fig. 2. However, if an electrical pulse of 800 ns and 0.22 V was applied to *a*-CASL, it changed to *m*-CASL instead of changing directly to *c*-CASL, (c) in Fig. 2. Then *m*-CASL changed to *c*-CASL by an electrical pulse of 800 ns and 0.28 V, (d) in Fig. 2. The contact resistance ranges from 175 to 250  $\Omega$  throughout the transitions. Thus its effect on the large resistance change (150 k $\Omega$ ) during state transition as illustrated in Fig. 2 can be ignored. The states can be triggered not only by the specific electrical conditions provided above. In fact, a certain range of electrical conditions can be used.

Two hundred times of reversible transitions in states have been obtained by using electrical pulses. The number of reversible transitions is dependent on the methods used for state transition, condition of the methods, and CASL structures. It can be improved by optimizing the above factors.

During phase transition there is stress change between the layers due to the volume change of amorphous and crystalline phases. However, it was reported that only about 9% of stress change was found for  $\text{Ge}_2\text{Sb}_2\text{Te}_5$  materials with a volume change of 7% [10]. A considerable fraction of the stress in the phase change film is relieved by plastic flow in the amorphous phase. In this work, the density change is about 7.8%. As  $\text{Ge}_2\text{Sb}_2\text{Te}_5$  can be viewed as a pseudobinary system of GeTe and  $\text{Sb}_2\text{Te}_3$ , it can be expected that the stress change is of similar level as reported [10] and thus is not a major factor of transition numbers.

Because of the three states, CASL can demonstrate three different physical properties. In this work the electrical, optical, thermal, and phase transition properties of CASL are discussed.

In principle, the theories developed for crystalline and amorphous SLs are suitable for describing the electronics properties of CASL. The in-plane of *m*-CASL can be viewed as a two dimensional system. The electrons or holes have quantized energy levels for one spatial dimension, but are free to move in two spatial dimensions. Our electrical conductivity measurement at lower temperature has confirmed this prediction. The wave vector is a good quantum number for two dimensions but not for the third dimension.

SL is optically equivalent to a uniaxial material with optical axis normal to the surface and with both ordinary and extraordinary optical constants. With the different states, CASL can provide three uniaxial materials with three ordinary and three extraordinary optical constants.

The optical properties of CASL at different states were studied by measuring normal incident reflection and trans-

mission that are determined by the ordinary refractive index  $n_o$  in the range of 0.4 to 1.2 eV. The values of the bandgap as a function of the component thickness were measured for the CASL at different state. Figure 3 shows the absorption edge values that were influenced by quantum well confinement for layer thickness less than 10 nm obtained for *m*-CASL. The blueshift of absorption edge was obviously observed. Similar blueshifts were also observed for *c*-CASL and *a*-CASL. The absence of any concrete information about the modulation profiles of the valence and conduction band edges, or about electron and hole effective masses, prevents an exact comparison of the measured blueshift with calculation. Nevertheless, the magnitude of the shift and the layer thickness values at which it sets in can be modeled with a square-wave modulation of band edge [11]. This model demonstrates that the variation in blueshift with layer thickness is indeed a quantum size effect.

Recently thermal properties of SL have attracted increasing attention due to the requirements of thermal control of properties in semiconductor devices. Significant reductions in both in-plane and cross-plane thermal conductivities of SLs have been observed theoretically and experimentally [12–14]. Because of the three states, CASL has three different thermal conductivities. It thus would offer a promising method for artificially synthesizing novel materials with different thermal properties. The thermal conductivity of CASL is highly dependent on the component film thickness and ratio. The measured thermal conductivity of *c*-CASL with a period of 7 nm is less than 30% of that of single layer bulk material.

CASL also demonstrates unique phase transition behavior. Because of different  $T_x(c)$  of the component materials, it has different crystallization mechanisms at *a*-CASL and

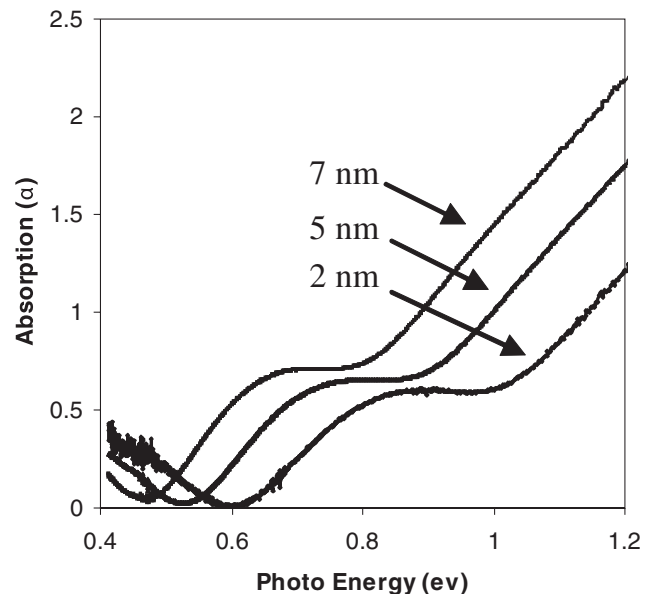


FIG. 3. Blueshift of absorption edges in *m*-ACSL state.

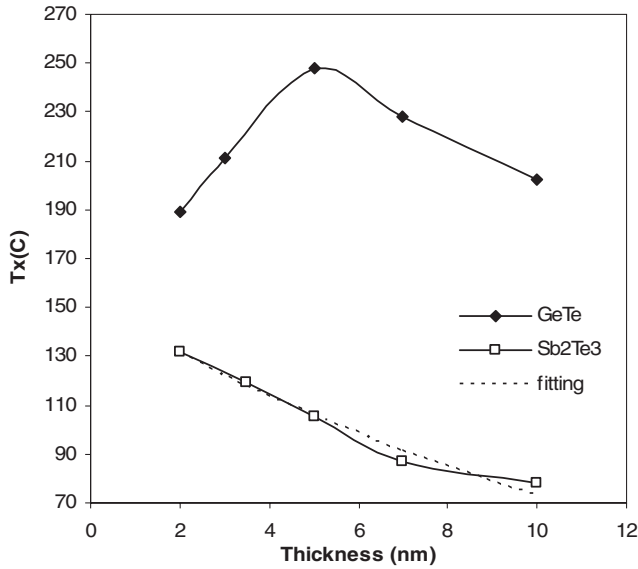


FIG. 4.  $T_x(c)$  of  $\text{Sb}_2\text{Te}_3$  sandwiched by GeTe as a function of layer thickness of  $\text{Sb}_2\text{Te}_3$ , and  $T_x(c)$  of GeTe sandwiched by  $\text{Sb}_2\text{Te}_3$  as a function of layer thickness of GeTe.

*m*-CASL states. The component material with lower  $T_x(c)$  crystallizes firstly through nucleation and growth process. It serves as a seed bed to induce a surface growth when another material starts to crystallize. In GeTe/ $\text{Sb}_2\text{Te}_3$  CASL, because  $T_x(c)$  of bulk  $\text{Sb}_2\text{Te}_3$  and GeTe materials is 100 °C and 200 °C, respectively, at *a*-CASL state  $\text{Sb}_2\text{Te}_3$  crystallizes firstly and subsequently functions as a seed bed at *m*-CASL state.

It has been found that  $T_x(c)$  is strongly dependent on the capping layer materials and their thicknesses [15]. The thickness dependence on  $T_x(c)$  of GeTe and  $\text{Sb}_2\text{Te}_3$  was measured. Figure 4 shows  $T_x(c)$  of GeTe sandwiched by  $\text{Sb}_2\text{Te}_3$  as a function of layer thickness of GeTe, and  $T_x(c)$  of  $\text{Sb}_2\text{Te}_3$  sandwiched by GeTe as a function of layer thickness of  $\text{Sb}_2\text{Te}_3$ . It can be seen that  $T_x(c)$  of  $\text{Sb}_2\text{Te}_3$  almost decreases exponentially with the increase in layer thickness. However,  $T_x(c)$  of GeTe increases firstly with its increase in thickness and reaches the maximum  $T_x(c)$  at about 5 nm. Then  $T_x(c)$  decreases with further increase in thickness.

It was reported that  $T_x(c)$  of amorphous Si/ $\text{SiO}_2$  SL is strongly enhanced by the presence of oxide interfaces.  $T_x(c)$  increases rapidly with the decreasing Si layer thickness. A model was developed to take into account of the interfacial energies, the layer thickness, melting point of the system, and  $T_x(c)$  of the thick amorphous layer [15]. In this work, this model was modified to describe the crystallization of component material with lower  $T_x(c)$  for *a*-CASL by introducing amorphous and polycrystalline phases,  $a_1$  and  $c_1$  for the component material with lower

$T_x(c)$ , respectively, and  $a_2$  and  $c_2$  for another component material, respectively. Based on the modification, an exponential increase of  $T_x(c)$  of  $\text{Sb}_2\text{Te}_3$  with decreasing layer thickness  $d$  can be derived

$$\begin{aligned} T_{c1} &= T_{a1c1} \left( 1 + \frac{\gamma_{a2c1} - \gamma_{a1c1} - \gamma_{a2a1}}{\gamma_{a1c1}} \right) e^{-d/4l_0} \\ &= AT_{a1c1} e^{-d/4l_0}, \end{aligned} \quad (1)$$

where  $T_{a1c1}$  is  $T_x(c)$  of bulk  $\text{Sb}_2\text{Te}_3$ ,  $\gamma_{a1c1}$ ,  $\gamma_{a2c1}$ , and  $\gamma_{a2a1}$  are interfacial free energies per unit area between amorphous  $\text{Sb}_2\text{Te}_3$  and polycrystalline  $\text{Sb}_2\text{Te}_3$  phases, between amorphous GeTe and polycrystalline  $\text{Sb}_2\text{Te}_3$  phases, and between amorphous GeTe and amorphous  $\text{Sb}_2\text{Te}_3$  phases, respectively,  $l_0$  is an average screening or bonding length related to the range of interatomic forces typical for amorphous GeTe and polycrystalline  $\text{Sb}_2\text{Te}_3$ . The simplified Eq. (1) was used to fit the experimental data by using  $A$  and  $l_0$  as the fitting parameters. The fitted result in Fig. 4 shows a good agreement with the experimental observations. When GeTe thickness is smaller than 5 nm, the trend of  $T_x(c)$  relates to the effect of surface induced growth caused by crystallized  $\text{Sb}_2\text{Te}_3$ .

In summary, a new class of semiconductor SL, CASL with three different states, *a*-CASL, *c*-CASL, and *m*-CASL has been proposed and demonstrated in this work. The optical, electrical, thermal, and phase transition properties of CASL can be designed and controlled by using different component materials and CASL structures. It enables the design and manipulation of materials with specific properties, and provides a promising method for synthesizing novel semiconductor material structure artificially.

\*shi\_luping@dsi.a-star.edu.sg

- [1] L. Esaki and R. Tsu, IBM J. Res. Dev **14**, 61 (1970).
- [2] B. Abeles and T. Tiedje, Phys. Rev. Lett. **51**, 2003 (1983).
- [3] N. Mott, Nobel Lecture, Physics 403 (1977).
- [4] S.R. Ovshinsky, Phys. Rev. Lett. **36**, 1469 (1976).
- [5] S.K. Bahl and K.L. Chopra, J. Appl. Phys. **41**, 2196 (1970).
- [6] S.A. Baily and D. Emin, Phys. Rev. B **73**, 165211 (2006).
- [7] S.H. Lee *et al.*, Appl. Phys. Lett. **89**, 223116 (2006).
- [8] Y.J. Wu *et al.*, Jpn. J. Appl. Phys. **38**, 1701 (1999).
- [9] B. Liu *et al.*, Microelectron. Eng. **82**, 168 (2005).
- [10] T.P.L. Pedersen *et al.* Appl. Phys. Lett. **79**, 3597 (2001).
- [11] A. Bittar *et al.*, Physica (Amsterdam) **157A**, 411 (1989).
- [12] S. Y. Renand and J. D. Dow, Phys. Rev. B **25**, 3750 (1982).
- [13] T. Yao, Appl. Phys. Lett. **51**, 1798 (1987).
- [14] R. Venkatasubramanian, Phys. Rev. B **61**, 3091 (2000).
- [15] M. Zacharias and P. Streitenberger, Phys. Rev. B **62**, 8391 (2000).